CrossMark

Piezoelectric sensor location by the observability Gramian maximization using topology optimization

Odair Menuzzi[1] · **Jun S. O. Fonseca[2]** · **Eduardo A. Perondi[2]** ·
Juliano F. Gonçalves[2] · **Eduardo Padoin[3]** · **Otávio A. A. Silveira[4]**

Abstract This work presents an optimal design methodology for piezoelectric material positioning in structures aiming at vibration measurements. The main objective is to find the optimal location of piezoelectric sensors using a suitable topology optimization strategy. The sensors location is determined by an optimization formulation that defines where the material should have piezoelectric properties. The objective of the optimization is maximizing observability, measured by means of the trace of the Gramian matrix. The control strategy development is based on a truncated modal system model. A case study and its results are presented and discussed, showing that the optimal placement of the piezoelectric sensors in a cantilever beam can be suitably achieved through the proposed approach.

Keywords Sensor placement · Observability Gramian · Topology optimization ·
Piezoelectric material

Mathematics Subject Classification 65K10 Optimization and variational techniques ·
93Bxx Controllability, observability, and system structure

✉ Odair Menuzzi
odair.menuzzi@iffarroupilha.edu.br

1 Farroupilha Federal Institute of Education, Science and Technology, Rua Otaviano Castilho Mendes 355, São Borja, RS 97670-000, Brazil

2 Department of Mechanical Engineering, Federal University of Rio Grande do Sul, Sarmento Leite 425, Porto Alegre, RS 90050-170, Brazil

3 Farroupilha Federal Institute of Education, Science and Technology, Rodovia RS-377, Alegrete, RS 97555-000, Brazil

4 Department of Civil Engineering, Federal University of Santa Catarina, Rua João Pio Duarte da Silva 205, Florianópolis, SC 88040-970, Brazil

🙂 Springer 〽BMAC

1 Introduction

Structures equipped with actuators, sensors and control systems have been the subject of study of many researches lately. These systems behave as intelligent structures (Gawronski 2004) and are widely studied due to the applications in the aerospace industries, but not least important in fields such as automotive, bio-medical and robotics (Schwantz 2002). Usually, the objective is to increase the dynamic performance using structures that have the ability of self-monitoring and active control. Piezoelectric sensors/actuators are extensively used for active control, since piezoelectric materials have suitable electromechanical properties, fast response, easy manufacturing, low weight, large operating bandwidth and no generation of magnetic field while converting electrical energy into mechanical energy (Gupta et al. 2010). In this context, the application of advanced techniques to the study and improvement of the existing projects is important. Thus, methods such as topology optimization contribute to the search for concepts that satisfy some project requirements (Bendsoe and Sigmund 2013) while decreasing costs. However, reducing the weight and changing the structure damping can generate some problems, such as excessive vibration. So, it is interesting to use an active control scheme, since a feedback system has the ability of reducing the output sensitivity with respect to parameter changes.

This type of problem can be treated by means of the control strategy along with the mechanical modeling. Therefore, it is important to ensure that the mathematical model describes accurately the electromechanical behavior of such structures (Tzou and Tseng 1990; Qi et al. 1997; Balamurugan and Narayanan 2002; Wang 2004). The performance of active control systems depends on not only the control law, but also the number and appropriate location of sensors and actuators. Donoso and Bellido (2009) distributed piezoelectric sensors in circular plates with polar symmetry of the boundary conditions. The problem was treated as a linear optimization method based on the sensors' response, where the design variable was a binary function used to model the polarization profile of the piezoelectric layer. Wang et al. (2011) presented a study on the topology optimization of planar piezoelectric actuators assembled by repetitive patterns where the objective was maximizing an output displacement, and the constraints were the actuation energy and the material volume. Silveira et al. (2015) developed a design methodology for actuator location, using topology optimization for the controllability Gramian maximization and linear quadratic regulator (LQR) control for vibration reduction. Kang et al. (2011) investigated the combined structural optimization of two materials, considering the layout and distribution of the piezoelectric actuators by maximization of the nodal displacement. A two-phase material model with penalization is used in the topology optimization of the actuator elements. Other important publications can be to found in Lee (2011), Alvelid (2008), Carbonari et al. (2007), Goncalves et al. (2016) and Kumar and Narayanan (2008).

A suitable technique used to determine sensors' optimal location in structures is based on the observability measurements. In an important work in this field, Hać and Liu (1993) employed the generalized Hankel matrix, a function of the system controllability and observability, to develop an approach that allows to determine sensor location based on a given rank for the system observability matrix while satisfying modal test constraints. Gawronski and Lim (1996) showed that the decomposition of the Hankel singular values of sensor/actuator allows to evaluate each individual sensor and actuator in terms of the system controllability and observability. According to Qiu et al. (2007), optimal sensor locations results in the same problem structure of optimal actuator locations when we maximize the degree of controllability/observability using the H2 norm. The optimization can also be performed via

heuristics techniques, which are used to determine the optimal configuration of the actuators and sensors. Xu et al. (2013) studied the integrated use of the number/position optimization of the actuators and sensors, and the control parameters of the piezoelectric material in plates, using genetic algorithm (GA). Zorić et al. (2013) studied the optimization of the piezoelectric actuator/sensor size and location. The parameter optimization of the controller is performed separately, using a fuzzy optimization strategy based on the particle swarm optimization in which the criteria for optimal sizing and location of piezoelectric actuators and sensors are written in terms of the eigenvalues of the controllability Gramian matrix.

Based on these references, this work proposes the development of a topology optimization methodology for the distribution of piezoelectric sensors aiming at the observability Gramian maximization. Two material phases are considered in the topology optimization: an elastic isotropic material forms the structural part and a piezoelectric material composes the active part (sensors). The application of this kind of methodology is important, since the convenient location of transducers improve the performance of the control system (Kumar and Narayanan 2008). In this work, an electromechanical finite element is employed for the numerical modeling of the structure dynamics considering the piezoelectric effects. Then, the observability Gramian is derived for this kind of structure in the context of optimal control. The topology optimization formulation in presented, and the sensitivities are derived analytically. Finally, some numerical results are presented and discussed.

2 Finite element formulation

In this work, a smart structure is modeled as a three-dimensional solid subject to infinitesimal strains. The piezoelectric material used as actuators and sensors is modeled by the following constitutive equations (Moheimani and Fleming 2006):

$$\mathbf{T} = [\mathbf{c}^E]\mathbf{S} - [\mathbf{e}]^T\mathbf{E}, \tag{1}$$

$$\mathbf{D} = [\mathbf{e}]\mathbf{S} - [\boldsymbol{\epsilon}^S]\mathbf{E}, \tag{2}$$

where $\mathbf{T}$ and $\mathbf{S}$ are the mechanical stress and infinitesimal strain vectors, respectively; $\mathbf{E}$ and $\mathbf{D}$ are the electric field and electric displacement vectors; $[\mathbf{c}^E]$, $[\mathbf{e}]$ and $[\boldsymbol{\epsilon}^S]$ are elastic, piezo-electric coupling and dielectric coefficients, respectively. The piezoelectric matrix represents the coupling between the mechanical and electrical fields.

The Hamilton principle can be used to derive the finite element equations for piezoelectric structures. Using this approach, the global balance equations that govern an electromechanical system can be written as follows:

$$\mathbf{M}_{uu}\ddot{\mathbf{u}} + \mathbf{C}_{uu}\dot{\mathbf{u}} + \mathbf{K}_{uu}\mathbf{u} + \mathbf{K}_{u\phi}\boldsymbol{\phi} = \mathbf{f}, \tag{3}$$

$$\mathbf{K}_{u\phi}^T\mathbf{u} + \mathbf{K}_{\phi\phi}\boldsymbol{\phi} = \mathbf{q}, \tag{4}$$

where $\mathbf{u}$ is the structural displacement, $\boldsymbol{\phi}$ the electric potential, $\mathbf{M}_{uu}$ the structural mass matrix, $\mathbf{C}_{uu}$ the structural damping matrix, $\mathbf{K}_{uu}$ the structural stiffness matrix, $\mathbf{K}_{u\phi}$ the piezoelectric coupling matrix, $\mathbf{K}_{\phi\phi}$ the dielectric capacitance matrix, $\mathbf{f}$ the vector of external force and $\mathbf{q}$ the vector of electrical charge.

The electrical degrees of freedom can be classified as potential electrode $\boldsymbol{\phi}_{\mathrm{p}}$, grounded electrode $\boldsymbol{\phi}_{\mathrm{g}}$, and internal degrees of freedom $\boldsymbol{\phi}_{\mathrm{i}}$. The voltage of the grounded electrodes can be eliminated and the internal degrees of freedom can be rewritten by means of a static condensation as:

$$\mathbf{M}_{uu}\ddot{\mathbf{u}} + \mathbf{C}_{uu}\dot{\mathbf{u}} + \mathbf{H}_{uu}\mathbf{u} + \mathbf{H}_{up}\boldsymbol{\phi}_{\mathrm{p}} = \mathbf{f}, \tag{5}$$

$$\mathbf{H}_{up}^T\mathbf{u} + \mathbf{H}_{pp}\boldsymbol{\phi}_{\mathrm{p}} = \mathbf{q}, \tag{6}$$

where $\mathbf{H}_{uu}$ is the condensed global stiffness matrix, $\mathbf{H}_{up}$ the condensed global piezoelectric coupling matrix, and $\mathbf{H}_{pp}$ the condensed global dielectric capacitance matrix. More details related to the static condensation procedure can be found in Becker et al. (2006).

3 Control model

The electric degrees of freedom are considered as active and known, i.e., as inputs for the actuator in the control system. Assuming short-circuit configuration, both electrodes are grounded and, therefore, the electrical charges $\mathbf{q}_p$ generated by the structural deformation is:

$$\mathbf{q}_p = \mathbf{H}_{up}^T \mathbf{u}. \tag{7}$$

To reduce the computational cost, a truncated model is adopted, i.e., only some vibration modes are used to represent the structural behavior. It is well known, however, that deriving the control system using reduced models can cause problems in practical applications. It can lead to spillover instabilities: excitation of residual modes by the control actuation which results in problems in the system observation and pollute the sensor output. Nevertheless, one can assume that the lower order modes are the most excited and have more significance for the system. A truncated modal matrix $\boldsymbol{\Psi}$ is generated by transforming the generalized coordinates $\mathbf{u}$ into modal coordinates $\boldsymbol{\eta}$, where the displacement vector can be approximated by the superposition of the m first modes, according to $\mathbf{u} = \boldsymbol{\Psi}\boldsymbol{\eta}$. With this transformation, the system order is reduced to the number of modes that represent the model instead the number of finite element degrees of freedom.

The control system can be described in terms of the modal coordinates; then we can rewrite Eq. (5) as:

$$\ddot{\boldsymbol{\eta}} + 2\mathbf{Z}\boldsymbol{\Omega}\boldsymbol{\eta} = -\boldsymbol{\Psi}^T\mathbf{H}_{up}\boldsymbol{\phi}_p + \boldsymbol{\Psi}^T\mathbf{f} \tag{8}$$

and Eq. (6), considering the electrical charge $\mathbf{q}_p$ as the control system output $\mathbf{y}$, as:

$$\mathbf{y} = \mathbf{H}_{up}^T\boldsymbol{\Psi}\boldsymbol{\eta}, \tag{9}$$

where $\boldsymbol{\Omega}$ is the diagonal matrix of natural frequencies and $\mathbf{Z}$ is the diagonal matrix of modal damping for the m modes. To obtain the state-space model, the state vector is initially defined in terms of the truncated model displacements and velocities $\mathbf{x} = \{\boldsymbol{\eta} \quad \dot{\boldsymbol{\eta}}\}^T$. Thus, the open-loop system is given by first-order differential equation expressed in terms of the state variable vector as:

$$\dot{\mathbf{x}} = \mathbf{A}\mathbf{x} + \mathbf{B}_\phi\boldsymbol{\phi}_p + \mathbf{B}_u\mathbf{f} \tag{10}$$

$$\mathbf{y} = \mathbf{C}\mathbf{x}, \tag{11}$$

where $\mathbf{f}$ and $\boldsymbol{\phi}_p$ are the mechanical and electrical input vectors, respectively; the system matrix is given by $\mathbf{A}$, the mechanical and electrical input matrix are given by $\mathbf{B}_u$ and $\mathbf{B}_\phi$, respectively, and $\mathbf{C}$ is the output matrix:

$$\mathbf{A} = \begin{bmatrix} \mathbf{0} & \mathbf{I} \\ -\boldsymbol{\Omega}^2 & -2\mathbf{Z}\boldsymbol{\Omega} \end{bmatrix}, \qquad \mathbf{B}_u = \begin{bmatrix} \mathbf{0} \\ \boldsymbol{\Psi}^T \end{bmatrix} \tag{12}$$

$$\mathbf{B}_\phi = \begin{bmatrix} \mathbf{0} \\ -\boldsymbol{\Psi}^T\mathbf{H}_{up} \end{bmatrix} \qquad \mathbf{C} = \begin{bmatrix} \mathbf{H}_{up}^T\boldsymbol{\Psi} & \mathbf{0} \end{bmatrix}, \tag{13}$$

where $\mathbf{I}$ and $\mathbf{0}$ are the identity and null matrices, respectively.

It is important to remark that this methodology does not take into account parametric uncertainties that can appear in real applications. Usually, the mathematical models do not accurately represent the real dynamics and, therefore, the control system cannot operate as designed due to the presence of parametric errors (Peruzzi et al. 2016). More details related to nonlinear response analysis can be found in Marcelo Tusset et al. (2016) and Pereira et al. (2017).

3.1 Observability Gramian matrix

The controllability and observability concepts are particularly important in the state-space control system design. It provides information about the dynamic system, being the base for the study of control and estimation of the system variables. The observability measures the ability of a sensor configuration to provide the required information to estimate the system states (Preumont 2011).

A system is considered observable if any state $\mathbf{x}(t_0)$ can be determined from the observation of $\mathbf{y}(t)$ during a finite time interval $t_0 \leq t \leq t_1$. The system is completely observable if every state transition affects each one of the output elements (Gawronski 2004). Considering a system with n states, the observability matrix $\mathcal{O}$ is given by:

$$\mathcal{O} = \begin{bmatrix} \mathbf{C}^{\mathrm{T}} & \mathbf{A}^{\mathrm{T}}\mathbf{C}^{\mathrm{T}} & \dots & (\mathbf{A}^{\mathrm{T}})^{n-1}\mathbf{C}^{\mathrm{T}} \end{bmatrix}. \tag{14}$$

The system $(\mathbf{A}, \mathbf{C})$ is completely observable if the matrix $\mathcal{O}$ has full rank. Since the system is dual, the pair $(\mathbf{A}, \mathbf{C})$ is observable if $(\mathbf{A}^{\mathrm{T}}, \mathbf{C}^{\mathrm{T}})$ is controllable (Preumont 2011). The application of the observability concept presents some drawbacks. The binary nature states that the answer is always qualitative, i.e., the system is controllable or not. An alternative is the formulation by means of the Gramian matrix, since it can be used to define a quantitative measure of the observability (Gawronski 2004). Through the duality between the observability and controllability, it is known that the system is observable if the pair $(\mathbf{A}^{\mathrm{T}}, \mathbf{C}^{\mathrm{T}})$ is controllable. Thus, the system is observable if the observability Gramian

$$\mathbf{W}_o = \int_0^\infty \exp\left(\mathbf{A}^{\mathrm{T}}\tau\right) \mathbf{C}^{\mathrm{T}}\mathbf{C} \exp\left(\mathbf{A}\tau\right) \, \mathrm{d}\tau \tag{15}$$

is positive definite (Preumont 2011). Alternatively, the observability Gramian can be obtained by the Lyapunov equation. Therefore, if $\mathbf{A}$ is stable asymptotically, $\mathbf{W}_o$ is defined as:

$$\mathbf{A}^{\mathrm{T}}\mathbf{W}_o + \mathbf{W}_o\mathbf{A} + \mathbf{C}^{\mathrm{T}}\mathbf{C} = \mathbf{0}. \tag{16}$$

According to Preumont (2011), the observability Gramian $\mathbf{W}_o$ reflects the ability of a non-zero state vector of initial conditions in affecting the system output.

4 Topology optimization

The optimization is defined as a set of procedures aiming to minimize or maximize a function, while obeying a set of constraints. In particular, the topology optimization aims to find the material distribution in a fixed domain. The location and size optimization of piezoelectric material in a structure was studied in several works (Kumar and Narayanan 2008; Lin et al. 2011; Wang et al. 2011; Xu et al. 2013). This work proposes a topology optimization design for piezoelectric material location in a structure, following an objective function written as the trace of the observability Gramian. The choice of measuring observability by the trace of the Gramian is justified by the fact that the Gramian matrix is diagonally dominant. Thus, the optimization problem is written as:

$$\max_{\boldsymbol{\rho}} \quad f = \text{trace} \left(\mathbf{W}_o \right), \tag{17}$$

$$\text{subject to} \begin{cases} 0 < \rho_i \leq 1 \\[2mm] \dfrac{V_s}{V} \leq C_s \end{cases}, \tag{18}$$

where ρ_i is the i-th component of the design variable vector with $i = 1, 2, \ldots n_e$, n_e is the number of design variable (number of finite elements), and the second constraint limits the total volume of piezoelectric material V_s following a threshold C_s.

4.1 Material model

The material model for topology optimization considers two solid phases: one is the isotropic elastic material and the other is the piezoelectric material. Therefore, the material model for the optimization problem with optimal location of piezoelectric material is given by:

$$\left[\mathbf{c}^E \right] = \rho^{p1} \left[\mathbf{c}_{\text{pzt}}^E \right] + \left(1 - \rho^{p1} \right) \left[\mathbf{c}_{\text{elas}}^E \right], \tag{19}$$

$$[\mathbf{e}] = \rho^{p2} \left[\mathbf{e}_{\text{pzt}} \right], \tag{20}$$

$$\left[\boldsymbol{\epsilon}^S \right] = \rho^{p2} \left[\boldsymbol{\epsilon}_{\text{pzt}}^S \right], \tag{21}$$

$$\gamma = \rho \gamma_{\text{pzt}} + (1 - \rho) \gamma_{\text{elas}}, \tag{22}$$

where the effective properties of the interpolated material are: the elastic properties $\left[\mathbf{c}^E \right]$, the dielectric properties $\left[\boldsymbol{\epsilon}^S \right]$, the piezoelectric coupling properties $[\mathbf{e}]$, and the specific weight γ. $\left[\mathbf{c}_{\text{elas}}^E \right]$ and $\left[\mathbf{c}_{\text{pzt}}^E \right]$ are the elastic properties of elastic and piezoelectric material, respectively; $\left[\boldsymbol{\epsilon}_{\text{pzt}}^S \right]$ and $\left[\mathbf{e}_{\text{pzt}} \right]$ define the properties of dielectric and electromechanical coupling of the piezoelectric material, respectively; γ_{elas} and γ_{pzt} refer to the specific weight for each material. Additionally, ρ is the design variable for sensor location defined in each finite element; $p1$ and $p2$ are penalization exponents that define a nonlinear mapping of the properties of the multiphase material with respect to the design variable. The main justification of the penalization is the reduction of areas with intermediate mixtures of the two phases. Following this material model, one can observe that when $\rho = 1$ the obtained properties define a piezoelectric material, while $\rho = 0$ yields to an isotropic elastic material.

4.2 Sensitivity analysis

The derivative of the objective function or constraint with respect to the variable is called sensitivity analysis, and it allows the use of first-order optimization algorithms, which are usually more efficient than algorithms without derivative. This is an important step in the solution procedure, because it indicates the direction of search in the solution space. For the particular choice of objective function and constraints, it is possible to derive analytically the sensitivities.

The sensitivities of the material model with respect to the i-th design variable are given by:

$$\frac{\partial \left[\mathbf{c}^E \right]}{\partial \rho} = p1 \rho^{p1-1} \left(\left[\mathbf{c}_{\text{pzt}}^E \right] - \left[\mathbf{c}_{\text{elas}}^E \right] \right), \tag{23}$$

$$\frac{\partial\,[\mathbf{e}]}{\partial\rho} = p2\rho^{p2-1}\left[\mathbf{e}_{\mathrm{pzt}}\right],\tag{24}$$

$$\frac{\partial\left[\boldsymbol{\epsilon}^{S}\right]}{\partial\rho} = p2\rho^{p2-1}\left[\boldsymbol{\epsilon}_{\mathrm{pzt}}^{S}\right],\tag{25}$$

$$\frac{\partial\gamma}{\partial\rho} = \gamma_{\mathrm{pzt}} - \gamma_{\mathrm{elas}},\tag{26}$$

where all terms have been already defined.

The observability Gramian sensitivity with respect to the design variables can be obtained from the differentiation of the Lyapunov equation (16):

$$\mathbf{A}^{\mathrm{T}}\frac{\partial\mathbf{W}_{o}}{\partial\rho} + \frac{\partial\mathbf{W}_{o}}{\partial\rho}\mathbf{A} + \left(\frac{\partial\mathbf{A}^{\mathrm{T}}}{\partial\rho}\mathbf{W}_{o} + \mathbf{W}_{o}\frac{\partial\mathbf{A}}{\partial\rho} + \frac{\partial\mathbf{C}^{\mathrm{T}}}{\partial\rho}\mathbf{C} + \frac{\partial\mathbf{C}}{\partial\rho}\mathbf{C}^{\mathrm{T}}\right) = \mathbf{0}.\tag{27}$$

If the four last terms of Eq. (27) are known, then the observability Gramian sensitivity $\partial\mathbf{W}_{o}/\partial\rho$ is obtained solving a new Lyapunov equation. The sensitivities of the parameters in state-space $\mathbf{A}$ and $\mathbf{C}$ can be evaluated by:

$$\frac{\partial\mathbf{A}^{\mathrm{T}}}{\partial\rho} = \begin{bmatrix} \mathbf{0} & \mathbf{I} \\ -\frac{\partial\boldsymbol{\Omega}^{2}}{\partial\rho} & -2\mathbf{Z}\frac{\partial\boldsymbol{\Omega}}{\partial\rho} \end{bmatrix} \qquad \frac{\partial\mathbf{C}}{\partial\rho} = \left[\frac{\partial\mathbf{H}_{up}^{\mathrm{T}}}{\partial\rho}\boldsymbol{\Psi} + \mathbf{H}_{up}^{\mathrm{T}}\frac{\partial\boldsymbol{\Psi}}{\partial\rho} \quad \mathbf{0}, \right]\tag{28}$$

where the term $\partial\mathbf{H}_{up}^{\mathrm{T}}/\partial\rho$ is required. This term was obtained from the static condensation of the stiffness matrix:

$$\mathbf{H}_{up}^{\mathrm{T}} = \left(\mathbf{K}_{up} - \mathbf{K}_{ui}\mathbf{K}_{ii}^{-1}\mathbf{K}_{ip}\right)\mathbf{T}_{o}.\tag{29}$$

Therefore, this sensitivity is given by:

$$\frac{\partial\mathbf{H}_{up}^{\mathrm{T}}}{\partial\rho} = \frac{\partial\mathbf{K}_{up}}{\partial\rho}\mathbf{T}_{o} - \left(\frac{\partial\mathbf{K}_{ui}}{\partial\rho}\mathbf{K}_{ii}^{-1}\mathbf{K}_{ip} + \mathbf{K}_{ui}\frac{\partial\mathbf{K}_{ii}^{-1}}{\partial\rho}\mathbf{K}_{ip} + \mathbf{K}_{ui}\mathbf{K}_{ii}^{-1}\frac{\partial\mathbf{K}_{ip}}{\partial\rho}\right)\mathbf{T}_{o},\tag{30}$$

where $\mathbf{T}_{o}$ is the explicit transformation matrix (see Becker et al. 2006), $\mathbf{K}_{up}$ and $\mathbf{K}_{ui}$ refer to the portions of the coupling matrix $\mathbf{K}_{u\phi}$ with potential and internal electrical degrees of freedom, respectively. Thus, they can be obtained from the assembly of the matrices from each finite element:

$$\frac{\partial\mathbf{K}_{u\phi}^{e}}{\partial\rho} = \int_{\Omega^{e}}\mathcal{B}_{u}^{\mathrm{T}}\frac{\partial\,[\mathbf{e}]^{\mathrm{T}}}{\partial\rho}\mathcal{B}_{\phi}\,\mathrm{d}\Omega^{e}.\tag{31}$$

$\mathcal{B}_{u}$ is a matrix that relates displacements and strains, $\mathcal{B}_{\phi}$ is a matrix that relates electric field and voltage, and Ω^{e} is the element volume.

The derivative of $\mathbf{K}_{ii}^{-1}$ is given by:

$$\frac{\partial\mathbf{K}_{ii}^{-1}}{\partial\rho} = -\mathbf{K}_{ii}^{-1}\frac{\partial\mathbf{K}_{ii}}{\partial\rho}\mathbf{K}_{ii}^{-1}.\tag{32}$$

Finally, the derivatives of $\mathbf{K}_{ii}$ and $\mathbf{K}_{ip}$ are obtained from the assembly of the dielectric capacitance matrices from each element:

$$\frac{\partial\mathbf{K}_{\phi\phi}^{e}}{\partial\rho} = \int_{\Omega^{e}}\mathcal{B}_{\phi}^{\mathrm{T}}\frac{\partial\left[\boldsymbol{\epsilon}^{S}\right]}{\partial\rho}\mathcal{B}_{\phi}\,\mathrm{d}\Omega^{e}.\tag{33}$$

The sensitivities for the vibration modes and natural frequencies are omitted. See for instance Wu et al. (2007).

4.3 Optimization procedure

In this section, we present the numerical implementation proposed in this study. A flowchart of the optimization algorithm is presented in Fig. 1.

After loading the required data, the modal analysis is performed using a solid FE model implemented considering the formulation of a eight-node brick element.

The optimal design variables are calculated by means of linear programming (LP) algorithm. This algorithm requires the objective and constraint functions to be linear. Otherwise, they can be expressed by a Taylor series expansion truncated at the linear term. Therefore, additional side constraints (also called moving limits) should be considered for the design variables, since this approximation is only acceptable for an arbitrarily small neighborhood.

The convergence criteria take into account the values of design variables for the current (k) and previous iterations, as follows:

$$\max \left\{ \left| \boldsymbol{\rho}^{(k)} - \boldsymbol{\rho}^{(k-1)} \right| \right\} \leq t_\rho, \tag{34}$$

where t_ρ is a tolerance parameter.

5 Numerical examples

The optimization procedure was implemented in MATLAB. A cantilever beam with dimensions 600 mm × 150 mm × 20 mm (Fig. 2) was analyzed. This structure was modeled using 1800 eight-node brick isoparametric elements with one electrical and three mechanical degrees of freedom per node.

For this example, the choice of materials was aluminum for the structural part and PZT5A for piezoelectric sensing. The piezoelectric material polarization is considered in the z-direction for easier manufacturing, since the electrodes are placed in the lateral faces, and, therefore, it works in the d_{31} mode. The constitutive properties of the elastic material (aluminum) and the piezoelectric material (PZT5A) are presented in Table 1. These constants were obtained from Mecchi et al. (2004) and Rubio et al. (2009).

The piezoelectric sensor location was designed for models with one, two, and six independents electrodes, as presented in Fig. 3. In this figure, red areas represent the electrodes and yellow areas represent isolation between the electrodes, where the piezoelectric properties were neglected. As the number of electrodes increases, more independent system outputs are available and the controller performance can be improved. The greater the number of independent sensors, the more can the vibration modes be reconstructed. This work analyzed cases with models truncated in the first, second, and forth vibration mode, resulting in nine different cases.

Based on Vasques and Rodrigues (2006), the following values for the first modal damping ratios were used for the control analysis: 1.71, 0.72, 0.42, and 0.41%. For simplicity sake, only two-dimensional cases are considered; thus, the degrees of freedom in the z-direction in the central xy-plane are restricted. The methodology does not require this simplification, which was placed to reduce the computational effort. For the optimization project, the piezoelectric volume constraint was equal to 5%. The design variables are set initially in the feasible range of $\rho = 0.04$ for all elements. The stopping criterion is a minimum number of 10 iterations or a change lesser than 2% in the design variables between successive iterations. Cubic penalization exponents were used in the material model.
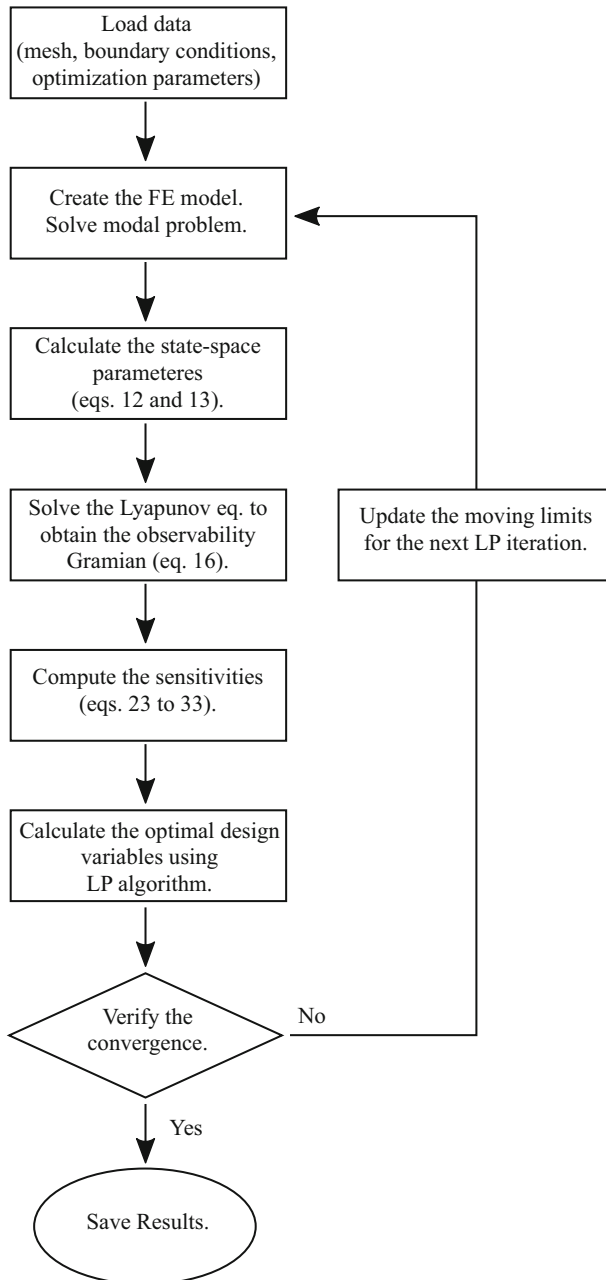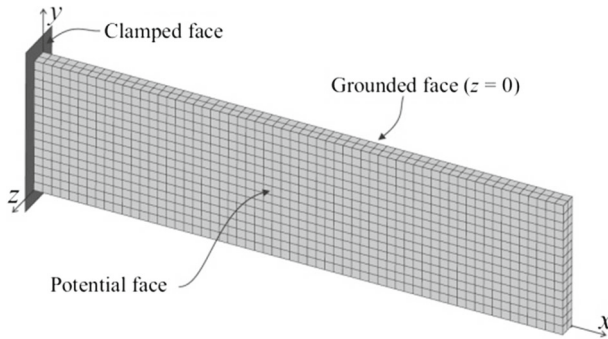
Fig. 1 Flowchart for the optimization process

Fig. 2 Three-dimensional cantilever beam

Table 1 Piezoelectric material properties	Elastic constant	$(10^{10}\ \text{N/m}^2)$
	c_{11}	12.10
	c_{12}	7.54
	c_{13}	7.52
	c_{33}	11.10
	c_{44}	2.11
	c_{66}	2.26
	Piezoelectric constant	(C/m^2)
	e_{31}	-5.4
	e_{33}	15.8
	e_{51}	12.3
	Dielectric constant	(F/m)
	ϵ_0	8.85×10^{-12}
	ϵ_{11}/ϵ_0	916
	ϵ_{33}/ϵ_0	830
	Density	7750 (kg/m^3)
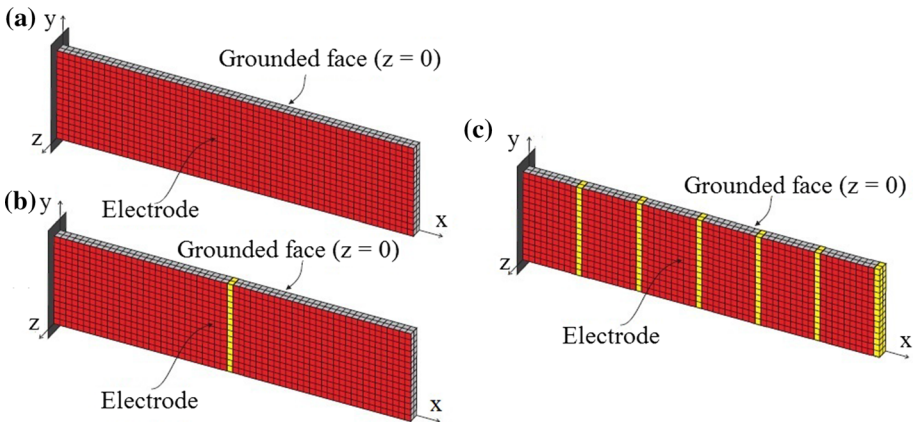
Fig. 3 Configuration of the potential electrodes: **a** one electrode, **b** two electrodes, and **c** six electrodes
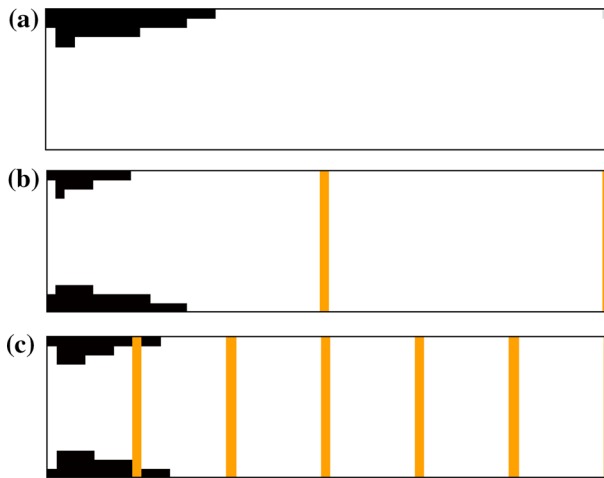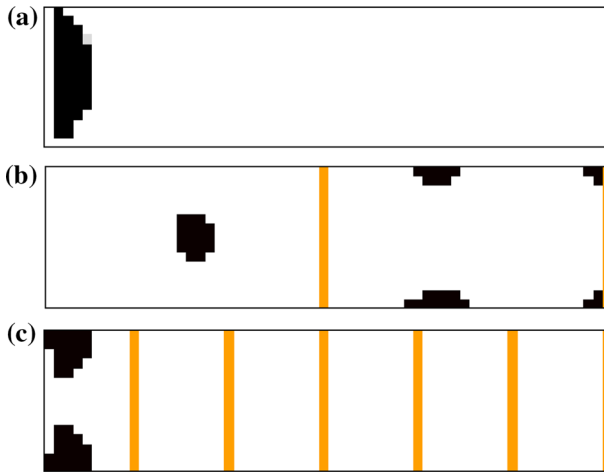
Fig. 4 Optimal topologies for piezoelectric material distribution for the first vibration mode. **a** One electrode, **b** two electrodes, and **c** six electrodes
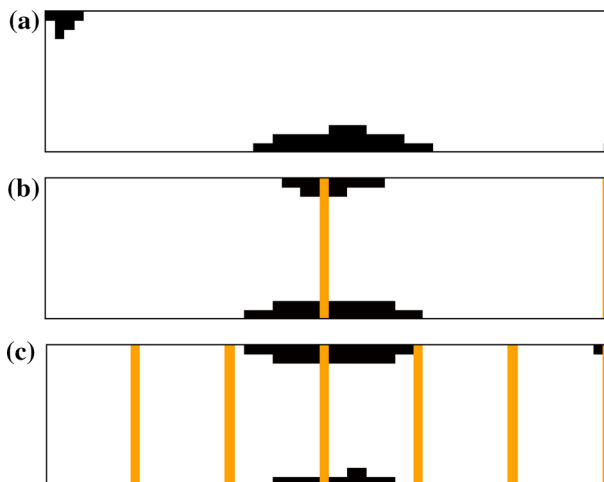
Fig. 5 Optimal topologies for piezoelectric material distribution for the second vibration mode. **a** One electrode, **b** two electrodes, and **c** six electrodes

5.1 Piezoelectric sensor location

The optimal topologies obtained from distribution of piezoelectric material for the first in-plane vibration mode are presented in the Fig. 4.

The optimal distribution of piezoelectric material for the second vibration mode and the cases with 1, 2, and 6 electrodes, respectively, are presented in Fig. 5.

The optimal distributions of piezoelectric material for the fourth vibration mode are presented in Fig. 6.

These results show that sensor location is related to the sensitivity of each analyzed mode. The convergence of the objective function is important to determine the optimization behavior

Fig. 6 Optimal topologies for piezoelectric material distribution for the fourth vibration mode. **a** One electrode, **b** two electrodes, and **c** six electrodes

Fig. 7 Objective function convergence for the first vibration mode with one electrode
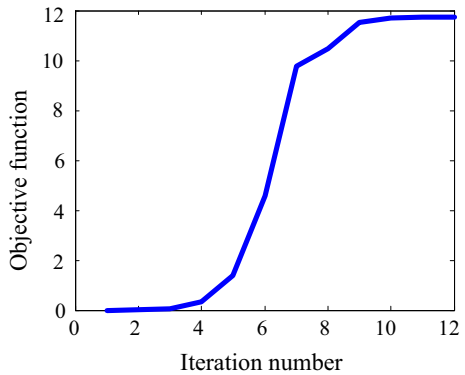
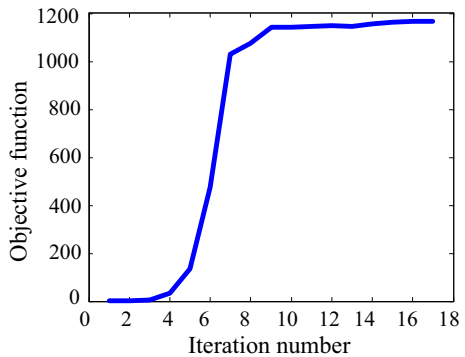**Fig. 8** Objective function convergence for the second vibration mode with two electrodes

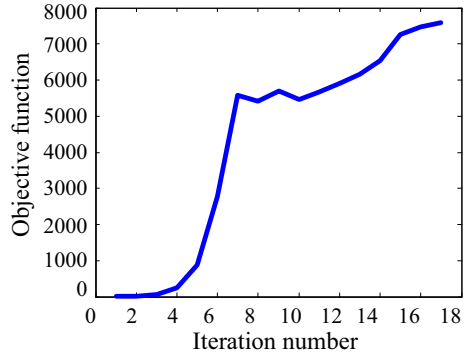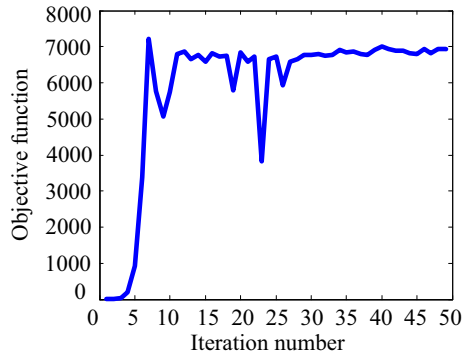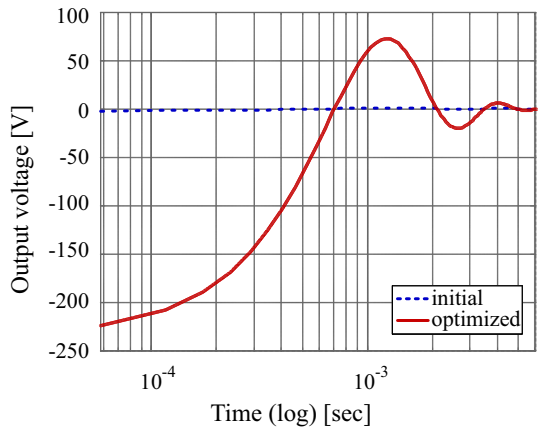**Fig. 9** Objective function convergence for the fourth vibration mode with one electrode

Fig. 10 Objective function convergence for the fourth vibration mode with six electrodes

Fig. 11 Output signal for the first vibration mode with one electrode

through the iterations. It is important to remark that the initial values of the design variable are equal for all cases. However, the objective function values are dissimilar due to distinct number of modes and electrodes for each case. The selected convergence histories are shown to demonstrate the convergence behavior of the optimization process. Figure 7 presents the objective function convergence history for the first vibration mode using one electrode, Fig. 8 shows this information for the second mode with one electrode, Fig. 9 the fourth mode with two electrodes, and Fig. 10 the fourth mode with six electrodes.

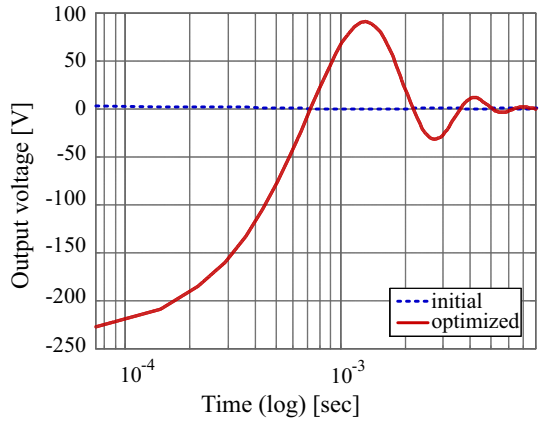**Fig. 12** Output signal for the first vibration mode with two electrodes

Fig. 13 Output signal for the second vibration mode with one electrode
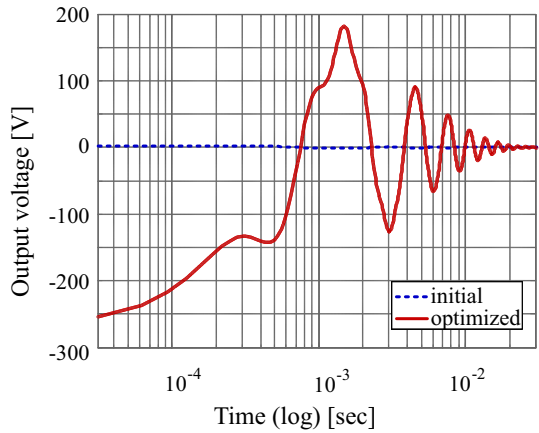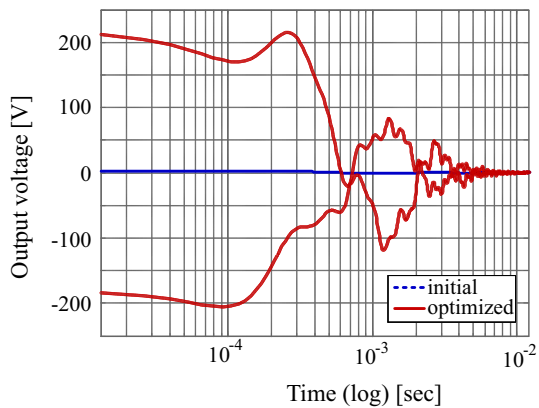

Fig. 14 Output signal for the fourth vibration mode with two electrodes

5.2 Sensor output signal

The output signals demonstrate significant improvement when compared with the starting point of the optimization process. Sensor signals were calculated considering the dynamic model described by the state-space equations (10) and (11), assuming an unit impulsive

load on the free-end of the cantilever beam. Figure 11 presents the output signal for the first vibration mode using one electrode. Figure 12 presents the output signal for the first vibration mode using two electrodes, while Fig. 13 shows this information for the second mode with one electrode, and Fig. 14 the fourth mode with two electrodes.

6 Conclusions

This work presented an optimum-based methodology for piezoelectric sensor location in structures by means of the observability Gramian. The results obtained by the application of this proposed formulation show that, through the maximization of the trace of observability Gramian, it was possible to increase the observability of the studied dynamic systems, improving the output signal sensor. When a larger number of vibration modes need to be reconstructed, a greater number of independent electrodes are required. The numerical results, presented in terms of the optimized topologies, objective function converges and output signals, also indicate that the number of electrodes used in the domain influences significantly the sensors location. The methodology is general and can be applied to mechanical structures with other materials and geometries.

References

Alvelid M (2008) Optimal position and shape of applied damping material. J Sound Vib 310(4):947–965

Balamurugan V, Narayanan S (2002) Finite element formulation and active vibration control study on beams using smart constrained layer damping (SCLD) treatment. J Sound Vib 249(2):227–250

Becker J, Fein O, Maess M, Gaul L (2006) Finite element-based analysis of shunted piezoelectric structures for vibration damping. Comput Struct 84(31):2340–2350

Bendsoe MP, Sigmund O (2013) Topology optimization: theory, methods, and applications. Springer Science and Business Media, New York

Carbonari RC, Silva EC, Nishiwaki S (2007) Optimum placement of piezoelectric material in piezoactuator design. Smart Mater Struct 16(1):207

Da Silveira OAA, Fonseca JSO, Santos IF (2015) Actuator topology design using the controllability gramian. Struct Multidiscip Optim 51(1):145–157

Donoso A, Bellido JC (2009) Distributed piezoelectric modal sensors for circular plates. J Sound Vib 319(1):50–57

Gawronski W (2004) Advanced structural dynamics and active control of structures. Springer Science and Business Media, New York

Gawronski W, Lim K (1996) Balanced actuator and sensor placement for flexible structures. Int J Control 65(1):131–145

Goncalves JF, Fonseca JS, Silveira OA (2016) A controllability-based formulation for the topology optimization of smart structures. Smart Struct Syst 17(5):773–793

Gupta V, Sharma M, Thakur N (2010) Optimization criteria for optimal placement of piezoelectric sensors and actuators on a smart structure: a technical review. J Intell Mater Syst Struct 21(12):1227–1243

Hać A, Liu L (1993) Sensor and actuator location in motion control of flexible structures. J Sound Vib 167(2):239–261

Kang Z, Wang R, Tong L (2011) Combined optimization of bi-material structural layout and voltage distribution for in-plane piezoelectric actuation. Comput Methods Appl Mech Eng 200(13):1467–1478

Kumar KR, Narayanan S (2008) Active vibration control of beams with optimal placement of piezoelectric sensor/actuator pairs. Smart Mater Struct 17(5):055008

Lee YS (2011) Comparison of collocation strategies of sensor and actuator for vibration control. J Mech Sci Technol 25(1):61–68

Lin ZQ, Gea HC, Liu ST (2011) Design of piezoelectric energy harvesting devices subjected to broadband random vibrations by applying topology optimization. Acta Mech Sin 27(5):730–737

Marcelo Tusset A, Piccirillo V, Bueno AM, Manoel Balthazar J, Sado D, Felix JLP, Brasil RMLRdF (2016) Chaos control and sensitivity analysis of a double pendulum arm excited by an rlc circuit based nonlinear shaker. J Vib Control 22(17):3621–3637

Mecchi ACL, Nader G, Silva ECN, Adamowski JC (2004) Development and characterization of a unimorph-type piezoelectric actuator applied to a michelson interferometer. Mechatronics 1(2):653–661

Moheimani SR, Fleming AJ (2006) Piezoelectric transducers for vibration control and damping. Springer Science and Business Media, New York

Pereira MdFV, Balthazar JM, dos Santos DA, Tusset AM, de Castro DF, Prado IAA (2017) A note on polynomial chaos expansions for designing a linear feedback control for nonlinear systems. Nonlinear Dyn 87(3):1653–1666

Peruzzi N, Chavarette FR, Balthazar JM, Tusset AM, Perticarrari ALPM, Brasil R (2016) The dynamic behavior of a parametrically excited time-periodic mems taking into account parametric errors. J Vib Control 22(20):4101–4110

Preumont A (2011) Vibration control of active structures: an introduction, vol 179. Springer Science and Business Media, New York

Qi H, Fang D, Yao Z (1997) Fem analysis of electro-mechanical coupling effect of piezoelectric materials. Comput Mater Sci 8(4):283–290

Qiu Zc, Zhang Xm, Wu Hx, Zhang Hh (2007) Optimal placement and active vibration control for piezoelectric smart flexible cantilever plate. J Sound Vib 301(3):521–543

Rubio WM, Silva EC, Paulino GH (2009) Toward optimal design of piezoelectric transducers based on multifunctional and smoothly graded hybrid material systems. J Intell Mater Syst Struct 20(14):1725–1746

Schwantz M (2002) Encyclopedia of smart materials. Wiley-Interscience Publication, New York

Tzou H, Tseng C (1990) Distributed piezoelectric sensor/actuator design for dynamic measurement/control of distributed parameter systems: a piezoelectric finite element approach. J Sound Vib 138(1):17–34

Vasques C, Rodrigues JD (2006) Active vibration control of smart piezoelectric beams: comparison of classical and optimal feedback control strategies. Comput Struct 84(22):1402–1414

Wang S (2004) A finite element model for the static and dynamic analysis of a piezoelectric bimorph. Int J Solids Struct 41(15):4075–4096

Wang X, Kang Z, Wang Y (2011) Topology design of slender piezoelectric actuators with repetitive component patterns. J Intell Mater Syst Struct 22(18):2161–2172

Wu B, Xu Z, Li Z (2007) A note on computing eigenvector derivatives with distinct and repeated eigenvalues. Int J Numer Methods Biomed Eng 23(3):241–251

Xu B, Ou J, Jiang J (2013) Integrated optimization of structural topology and control for piezoelectric smart plate based on genetic algorithm. Finite Elem Anal Design 64:1–12

Zorić ND, Simonović AM, Mitrović ZS, Stupar SN (2013) Optimal vibration control of smart composite beams with optimal size and location of piezoelectric sensing and actuation. J Intell Mater Syst Struct 24(4):499–526